Published in final edited form as:
J Biomed Mater Res A. 2015 April ; 103(4): 1303–1311. doi:10.1002/jbm.a.35202.

Real Time Visualization and Characterization of Platelet Deposition under Flow onto Clinically-Relevant Opaque Surfaces

Megan A. Jamiolkowski[1,2,*], **Joshua R. Woolley**[1,2,*], **Marina V. Kameneva**[1,2,3], **James F. Antaki**[2,5], and **William R. Wagner**[1,2,3,4]

[1]McGowan Institute for Regenerative Medicine, Pittsburgh, PA

[2]Dept. of Bioengineering, University of Pittsburgh, Pittsburgh, PA

[3]Dept. of Surgery, University of Pittsburgh, Pittsburgh, PA

[4]Dept. of Chemical Engineering, University of Pittsburgh, Pittsburgh, PA

[5]Dept. of Biomedical Engineering, Carnegie Mellon University, Pittsburgh, PA

Abstract

Although the thrombogenic nature of the surfaces of cardiovascular devices is an important aspect of blood biocompatibility, few studies have examined platelet deposition onto opaque materials used for these devices in real time. This is particularly true for the metallic surfaces used in current ventricular assist devices (VADs). Using hemoglobin depleted red blood cells (RBC ghosts) and long working distance optics to visualize platelet deposition, we sought to perform such an evaluation. Fluorescently labeled platelets mixed with human RBC ghosts were perfused across 6 opaque materials (a titanium alloy (Ti6Al4V), silicon carbide (SiC), alumina (Al_2O_3), 2-methacryloyloxyethyl phosphorylcholine polymer coated Ti6Al4V (MPC-Ti6Al4V), yttria partially stabilized zirconia (YZTP), and zirconia toughened alumina (ZTA)) for 5 min at wall shear rates of 400 and 1000 sec^{-1}. Ti6Al4V had significantly increased platelet deposition relative to MPC-Ti6Al4V, Al_2O_3, YZTP, and ZTA at both wall shear rates ($P < 0.01$). For all test surfaces, increasing the wall shear rate produced a trend of decreased platelet adhesion. The described system can be a utilized as a tool for comparative analysis of candidate blood-contacting materials with acute blood contact.

Keywords

platelets; thrombosis; red blood cell ghosts; opaque biomaterials; and ventricular assist device

Introduction

The implantation of several important cardiovascular devices, such as vascular grafts, stents, and cardiac valves, is associated with a risk of device-initiated thrombosis and

Address for correspondence: William R. Wagner, 450 Technology Dr., Suite 300, Pittsburgh, PA 15219, wagnerwr@upmc.edu.
*Author's contributed equally to the publication

thromboembolic events [1,2]. A substantial portion of biomaterials research has been devoted to developing methods to reduce the thrombogenicity of these devices through their design and surface manipulation [1–5]. Numerous reports have focused on developing inert, nonfouling materials to prevent platelet adhesion and subsequent thrombus formation. For example, the anticoagulant heparin has been immobilized through covalent bonding, ionic bonding, and physical adsorption [1–4]. To reduce platelet deposition onto common metallic biomaterials, coatings such as diamond like carbon (DLC) and 2-methacryloyloxyethyl phosphorylcholine (MPC) polymers have been investigated [2, 3, 5]. Although a wide array of approaches have been investigated to reduce material thrombogenicity, thrombosis complications remain of clinical significance for many devices. Thus surfaces with improved biocompatibility, as well as methods to quantify such improvements, remain of interest to the cardiovascular device community.

Amongst blood contacting devices, continuous flow ventricular assist devices (VADs) present particular blood biocompatibility challenges due to their complex blood flow pathways, supra-physiological shear rates, large blood contacting surface areas, and extended implant periods in patients with advanced cardiovascular disease. Consequently, the threat of thromboembolic events and pump thrombosis continues to be a major concern among implanting centers [2, 6–8]. A recent multicenter study by Starling et al. found that there has been an increase in device-related thrombosis in patients implanted with the Heartmate II VAD (Thoratec, Pleasanton, CA), one of the most widely used VADs and currently the only device of its kind to be FDA-approved for “destination therapy” (i.e. permanent implantation) [6, 9]. This increase was associated with substantial morbidity and mortality. The authors reported that the incidence of device-related thrombosis has increased from 2.2% in 2011 to 8.4% in 2013 [9]. A contributing factor for this complication may be recent trends of reducing the levels of anti-coagulation to decrease the incidences of gastro-intestinal bleeding [10].

The manufacturers of the Heartmate-II and other continuous flow VADs currently use a polished titanium alloy (Ti6Al4V) as the blood contacting surface due to its desirable mechanical properties, resistance to corrosion, and tolerable blood compatibility [11]. However, *in vitro* studies have shown that this alloy exhibited elevated acute thrombogenicity compared to other coated surfaces (e.g. polyethylene glycol and diamond-like coatings) or related alloys (Ti6Al7Nb) [2, 5, 12, 13]. This study was therefore conducted to perform a systematic side-by-side comparison of six candidate biomaterials currently being considered for application in continuous-flow blood pumps. However, since these materials are opaque, traditional methods for real time visualization of platelet deposition, such as fluorescent microscopy utilizing whole blood, are not readily applicable. The present study demonstrates a method to overcome this limitation through the use of a blood analogue containing *transparent*, hemoglobin depleted red blood cells (RBC ghosts) combined with fluorescently-labeled platelets. The experimental preparation consisted of a parallel plate flow chamber with epifluorescence microscopy having a long working-distance objective. This preparation permitted real-time observation of deposition and embolization to identify promising alternatives to Ti6Al4V to improve the overall blood compatibility of the device, reducing reliance on anticoagulation and anti-platelet agents.

Materials and Methods

Platelet Collection and Fluorescent Labeling

Fresh whole blood was collected after informed consent from 27 healthy donors (13 male, 14 female), who had refrained from taking any platelet altering medications 14 days prior to collection, with a mean age of 35±12 years in accordance with Institutional Review Board guidelines. Platelet-rich-plasma (PRP) was collected by centrifuging citrated blood (0.5 mL Vacutainer tubes, [0.105M] citrate, BD, Franklin Lakes, NJ, USA) at 250×g for 15 min. Platelets ($2.7 \pm 0.30 \times 10^8$ per mL) were fluorescently labeled by the addition of quinacrine dihydrochloride (0.5 μM final concentration, Sigma-Aldrich, St. Louis, MO, USA) to the PRP. Quinacrine dihydrochloride was chosen because studies have shown that platelet function is not affected when a final concentration < 20 μM is used [14, 15].

RBC Ghost Preparation and Characterization

Packed RBCs (type O-, Valley Biomedical Products & Services, Inc., Winchester, VA, USA) were converted into RBC ghosts through the modification of established protocols [16–19]. Briefly, the RBCs were rinsed and centrifuged (2000×g, 15 min) three times with phosphate buffered saline without Ca^{2+} or Mg^{2+} (PBS, VWR International LLC., Radnor, PA, USA) and then suspended in PBS at a 50% hematocrit. While incubated between 0–6°C, 1 mL of RBC suspension was added to every 9 mL of a lysing solution composed of 4mM $MgSO_4$, 5X concentrated PBS (25 mL per L distilled water), and acetic acid (Sigma-Aldrich, 80μL per L of distilled water) in distilled water with a final osmolality of 40 mOsm and pH of 5.0–5.2. After 5 min incubation, osmolality and pH were increased to physiologic norms (300 mOsm and 7.8, respectively) by the addition of 0.3 mL of 5X concentrated PBS and 2μL of 1M Tris buffer (Thermo Fisher Scientific Inc., Pittsburgh, PA, USA) per mL of cell suspension and stored at 0–6 degrees C for 8 hrs. The cells were then resealed by incubation at 37°C for 1 hr. The suspension was centrifuged at 25400×g for 30 min and the supernatant was discarded. The cells were washed 3 times with PBS (25400×g for 30 min) and stored in PBS with 100 mg/L gentamicin (Thermo Fisher Scientific). The resulting RBC ghosts were observed to be translucent. The donor PRP was utilized within 6 hr after being drawn to minimize platelet activation. Therefore RBC ghosts were prepared prior to the blood draw and added to the donor PRP. Blood type O^- RBCs were used to create RBC ghosts cells to allow mixing with any donor PRP blood type. The RBC ghosts were stored up to 2 wk at 4–6°C and a final hematocrit of ≥ 95%. These cells were utilized in the perfusion experiments within this time.

Prior to RBC ghost creation, an aliquot of native RBCs was set aside for comparative rheological testing. The viscosity of RBC ghosts in human plasma was measured using a cone and plate viscometer (Brookfield Digital Rheometer, Model DV-III, Brookfield Engineering Laboratories, Inc., Stoughton, MA, USA) and compared to native RBCs at the same hematocrit. The elongation of RBC ghosts and native RBCs at various wall shear rates was measured using an optical rheology system (CSS-450, Linkam Scientific Instruments Ltd., Tadworth, Surrey, UK) and analyzed using ImageJ (NIH). The elongation index was calculated as (L−W)/(L+W) where L and W are the major and minor axes of the ellipse representing elongated RBC, respectively.

Test Materials

Ti6Al4V and 5 alternative materials or coatings were analyzed: Ti6Al4V (Supra Alloys Inc., Camarillo, CA, USA), a modified 2-methacryloyloxyethyl phosphorylcholine polymer coated Ti6Al4V (MPC-Ti6Al4V), silicon carbide (SiC; CoorsTek, Inc., Golden, CO, USA) alumina (Al_2O_3; CoorsTek), yttria partially stabilized zirconia (YZTP; CoorsTek), and Zirconia Toughened Alumina (ZTA; CoorsTek). All the materials had a mirror polish finish. MPC-TI6AL4V was prepared in the authors' laboratory using previously reported protocols [4]. The materials evaluated were selected for their physical characteristics, which were generally compatible with use as blood contacting materials in a continuous flow VAD. A contact angle goniometer (VCA optima, AST Product Inc., Billerica, MA) was used to measure the contact angle of 1 μL of distilled water at room temperature on each surface. All samples were cleaned with Simple Green® (Thermo Fisher Scientific Inc.) and Tergazyme® (Alconox, Inc., White Plains, NY, USA) and then sonicated three times with distilled water prior to testing using a protocol based on the cleaning methods utilized for continuous flow VADs undergoing preclinical testing [20].

Parallel Plate Flow Chamber

The parallel plate flow chamber design was similar to that described by Kent et al. [21]. The top plate was clear acrylic with angled nylon inflow and outflow luer connectors, and the bottom plate was the interchangeable test material. A simple clamping mechanism held the plates together, with a silicone gasket outlining the channel width and length (5 × 8 mm). Aluminum shim stock was placed between the plates to provide a precisely defined channel height of 0.076 mm (Figure 1A–B). The flow within this chamber was assumed to be one-dimensional laminar parallel plate flow (Reynolds numbers between 0.1 and 0.4) [5, 21].

Blood Analogue Perfusion and Image Acquisition

The experimental flow path is presented in Figure 1C. All non-test surfaces were passivated by incubation with 1% bovine serum albumin (BSA, microbiological grade powder; MP Biomedicals, LLC, Solon, OH, USA) in PBS for 20 min prior to perfusion. To verify passivation, platelet deposition onto the acrylic top plate was qualitatively assessed after the perfusion experiments. Few to no adherent platelets were found. Quinacrine dihydrochloride - labeled PRP was mixed with RBC ghosts to produce an end hematocrit of 25% and a final platelet concentration of $2.0 \pm 0.2 \times 10^8$ platelets/mL. This suspension was collected into a 20 mL polystyrene syringe (BD Biosciences) and pulled through the parallel plate flow chamber by a syringe pump (Harvard Apparatus, Holliston, Massachusetts, USA) for 5 min at flow rates of 0.118 and 0.295 mL/min (wall shear rates of 400 sec^{-1} and 1000 $sec,^{-1}$ respectively). These wall shear rates were chosen to represent a low (400 sec^{-1}) and high (1000 sec^{-1}) physiological rate. Continuous flow VADs produce a wide range of wall shear rates within the pumps, including supra-physiological wall shear rates of >25000 sec^{-1} (shear stress > 100 N/m^2) [22–24]. However, the wall shear rates represented in this study are characteristic of those produced within the inlet and outlet regions and along the outer wall of centrifugal VADs (e.g. the clinically utilized HeartWare) [22, 23] and near the inlet in a region called the inducer in axial flow VADs (e.g. the clinically utilized HeartMate II) [24].

Platelet adhesion was visualized within a 200×200 micron region of interest, located 4 mm downstream from the inlet connector, in real time, using an inverted epifluorescence microscope (Olympus IX FLA, Olympus Corporation, Shinjuku, Tokyo, Japan) with a 40x super long working distance objective (PlanFL, phase contrast, working distance 6.5 mm – 8.3 mm, numerical aperture 0.55, and maximum acceptable coverslip thicknesses of 2.6 mm; Olympus Corporation) and a 103W HBO short arc mercury lamp light source (OSRAM GmbH, Munich, Germany). Images were acquired every 0.4 sec beginning at one min after the start of perfusion using a CCD camera (PCO-TECH Inc., Romulus, Michigan, USA).

Images were analyzed by thresholding the intensity, subjectively to eliminate spurious artifacts (See Figure 2A and 2B.). The surface coverage (in percent) of deposited platelets was computed using a custom written program in MatLab (MathWorks, Inc., Natick, MA, USA). To visually determine the accuracy of the analysis the outline of the original image was overlaid onto the original image (Figure 2C).

Scanning Electron Microscopy

Following perfusion, samples were gently rinsed with PBS and incubated with glutaraldehyde (2.5% in PBS; Sigma-Aldrich) for 10 min. Next, the materials were washed 3 times with PBS and dehydrated in consecutive stages of increasing ethanol (Sigma-Aldrich) concentrations. The samples were then chemically dried with hexamethyldisilazane (Thermo Fisher). Finally, the samples were coated with gold-palladium (Hummer VI Sputtering System, TechnicsWest, Inc., San Jose, California, USA) and scanning electron micrographs (SEMs) were obtained (images obtained using scanning electron microscope model JSM6330F, JEOL, Tokyo, Japan).

Flow Cytometry

Bulk phase activation of the platelets was measured by flow cytometry using previously described methods [25]. Briefly, blood was sampled from the exit port of the parallel plate chamber at two points in time: immediately after the sample initially crossed the test surface (determined visually) and also after 5 min perfusion. Aliquots of these samples were incubated in buffer solution (Tyrode's solution with 1% BSA, Electron Microscopy Science, Hatfield, PA, USA) with fluorescein isothiocyanate – conjugated mouse anti–human CD42b (CD42b, clone LG.3A10; AbDSerotec, Raleigh, NC, USA) and either recombinant phycoerythrin–conjugated (RPE) mouse anti-human CD62P or RPE-conjugated isotype-matched control antibody (CD62P and Mouse IgG_1, clones Psel.KO.2.5 and W3/25, respectively; both from AbDSerotec) in the dark for 20 min. The cells were washed with Tyrode's solution with 1% BSA and 0.106 M sodium citrate dehydrate (Thermo Fisher), centrifuged, and the pellet isolated. The cells were re-suspended in 1% paraformaldehyde (Sigma-Aldrich) and stored at 4° C (<24 hr) until analyzed. CD42b+ events (>5000) were collected on a 3-color FACScan (BD Biosciences) and analyzed with WINList software (Verity Software House, Topsham, ME).

Statistical Analyses

All data are presented as mean ± standard error of the mean. Data were analyzed by two-way, repeated measures ANOVA with specific post- hoc testing using the Bonferroni correction. SPSS v20 (IBM Corp, Armonk, NY) was used for all statistical analyses.

Results

RBC Ghost Rheology

To verify that flow behavior of RBC ghosts is similar to that of native RBCs, the rheological properties of RBC ghost suspensions were examined by comparing their viscosity as a function of shear rate to that of native RBCs used for the ghost preparation. Figure 3A depicts the viscosity response of native and ghost RBCs in plasma over a range of shear rates. No difference between the two curves was found (Figure 3A, P=0.61). Similarly, there was no difference found in deformability of the original RBCs and their ghosts (Figure 3B) and in their calculated elongation indices (Figure 3C; P = 0.41). Additionally, no significant difference in bulk phase platelet activation was detected between PRP and PRP mixed with RBC ghosts (8.7 ± 0.9% and 7.3 ± 0.9%, respectively; P=0.13, N=5).

Acute Platelet Adhesion on Test Surfaces

Representative fluorescent images of platelet adhesion onto the 6 opaque test surfaces after 5 min of perfusion at wall shear rates of 400 and 1000 sec^{-1} are shown in Figure 4. At the lower wall shear rate of 400 sec^{-1}, Ti6Al4V had 6.0% ± 2.0% (n=7) platelet deposition after 60 sec of perfusion, which continued to increase throughout the test resulting in platelet surface area coverage of 11.2 ± 1.6% (Figure 5). Similarly, SiC had 5.5% ± 1.2% (n=7) at 60 sec of perfusion which increased to 15.6 ± 2.2% in 5 min. Platelet adhesion onto Ti6Al4V and SiC increased significantly with time and were not different from each other ($P<0.05$). In contrast, Al_2O_3, YZTP, ZTA, and MPC-TI6Al4V all had significantly lower platelet adhesion ($P<0.005$) than the previous two surfaces, with average end platelet surface coverage of 3.3 ± 0.9%, 2.5 ± 1.1%, 1.3 ± 0.3%, and 1.2 ± 0.5%, respectively (Figure 5).

At the higher wall shear rate of 1000 sec^{-1}, all of the test materials had significantly less platelet adhesion than Ti6Al4V ($P<0.001$) (Figure 6). After 5 min perfusion, Ti6Al4V had platelet surface coverage of 4.8 ± 1.0%. In contrast, Al_2O_3, SiC, YZTP, ZTA, and MPC-TI6Al4V had average end platelet surface coverage of 1.2 ± 0.3%, 0.66 ± 0.35%, 0.60 ± 0.17%, 0.32 ± 0.13%, and 0.63 ± 0.23%, respectively.

Representative real-time perfusion videos of platelets adhering to all six surfaces, at wall shear rates of 400 or 1000 sec^{-1}, are available in the Supplemental Material (Figure S2–13). Although all materials had visible platelet deposition present during the experiments, the most pronounced thrombi formations were clearly observed with the Ti6Al4V samples at high and low wall shear rates and SiC samples at low wall shear rates. The thrombi grew in elliptical patterns, with the long axis aligned in the direction of flow. Embolization of fragments and entire thrombi were observed sporadically with the Ti6Al4V, SiC, Al_2O_3, and YZTP samples. Examination of the length of the flow path following perfusion indicated

that platelets reacted uniformly with the test materials and were not diffusion-limited by the rapid depletion of platelets onto the surface at the inlet of the chamber [26].

Wall Shear Rate Effect on Platelet Adhesion

Curves comparing platelet adhesion to each of the six test surfaces at the two wall shear rates are presented in the supplemental material (Figure S1). Increasing the wall shear rate from 400 to 1000 sec^{-1} produced a trend of decreased platelet adhesion to the test surfaces. This trend was significant for all of the surfaces, except MPC-Ti6Al4V ($P<0.05$). The largest change in platelet adhesion between wall shear rates occurred with SiC, in which a 95 ± 2% decrease in platelet surface coverage was observed at t = 5 min at the higher perfusion rate.

Surface Contact Angles, Scanning Electron Microscopy and Flow Cytometry

Water contact angles of the materials measured prior to use were as follows; Ti6Al4V: 55.3 ± 3.1°, SiC: 72.14 ± 3.6°, Al2O3: 69.2 ± 2.7°, YZTP: 31.3 ± 2.0°, ZTA: 42.0 ± 2.1°, and MPC-Ti6AL4V: 20.6 ± 2.1°.

Scanning electron micrographs of platelet deposition following blood analogue perfusion revealed similar adhesion patterns on the material surfaces as shown in the fluorescent images (Figure 7). Similar to the fluorescent images, the scanning electron micrographs revealed oval thrombi aligned in the direction of flow on the Ti6Al4V at both wall shear rates and on SiC at a wall shear rate of 400 sec^{-1}. Also, these micrographs verify that there is substantially less platelet deposition on the four other test surfaces. From the flow cytometry data, there was no difference found between materials or over the course of the perfusions in bulk phase platelet activation or circulating platelet-platelet microaggregate formation ($P > 0.25$). The average percent of activated platelets and microaggregates across all of the materials at both time points were 8.0 ± 2.1% and 1.2 ± 0.3% respectively.

Discussion

Characterization of the *in vitro* thrombogenicity of surfaces is an important step in developing and selecting new materials for use in blood-wetted devices. Previous methods for examining acute platelet deposition have utilized end-point analysis [27, 28], required that the material be transparent [29] or have used PRP instead of blood to perfuse over the surfaces [30]. The use of RBC ghosts mixed with PRP allows for a more physiologically relevant analysis of platelet deposition. Native RBCs have been shown to be involved in the transport of platelets to the vessel wall [17]. When blood flows through the microvessels the RBCs migrate towards the center of the vessels, crowding the platelets outward and increasing their concentration at the vessel wall [17, 31]. This phenomenon has also been observed with *in vitro* flow systems, where the increased platelet gradient near the test surfaces enhances platelet-surface interactions and increases the likelihood of platelet adhesion [31, 32]. A recent computational model of platelet adhesion in shear flow suggests that platelet adhesion is dependent upon near-wall collisions with RBCs [33].

The axial migration of RBCs that promotes platelet transport away from the center of vessels is also dependent on the unique abilities of RBCs to deform and aggregate [34, 35].

The combination of aggregation and the deformability of RBCs are also responsible for the shear-thinning characteristics of whole blood [36]. Because the ghost RBCs produced in this study had an identical viscosity curve and deformability as native red blood cells, they are expected to produce the same transport phenomena. Therefore, optically clear RBC ghosts were deemed acceptable substitutes for native RBCs in order to maintain the increased platelet concentration near the chamber walls while producing a transparent test fluid.

A parallel plate microfluidic device was chosen for this study because it provided one-dimensional, laminar flow and a defined wall shear rate [5, 21]. Szarvas et al. [37] found the parallel plate flow chamber to be superior to the cone and plate viscometer as the latter reduced surface-specific platelet deposition and experienced an increased reduction in single platelets with time. Other studies have utilized commercially available rotating disk or modified cone and plate viscometer systems to examine platelet adhesion to artificial surfaces with a wall shear stress gradient along the diameter of the disk or plate [38–41]. However, real-time videos of platelet deposition on opaque surfaces using whole blood with these systems have not yet been described. Uchida et al. [39] used a cone and plate viscometer to show that time dependent platelet adhesion could be reduced by coating commercially pure titanium with apatite, and apatite composites. However, images were only acquired every 5 min for a total of 15 min and PRP was utilized instead of whole blood [39]. Furukawa et al. [41] modified a cone and plate viscometer with transparent quartz glass which allowed for real time imaging of epifluorescent platelet deposition onto clear and opaque materials. However, PRP was still used as the perfusion fluid [41].

Schaub et al. previously presented a method for visualization of time-dependent platelet deposition on opaque surfaces [5]. In that report platelet deposition was measured on opaque metallic and polymeric materials at discrete time points by introducing into the fluid path a fiber optic bundle coupled to an epifluorescent microscope. However, this technique allowed for only brief periodic visualization of platelet adhesion with a limited field of view (100 μm diameter). Additionally, each time the fiber optic bundle was inserted into the chamber it altered the fluid dynamics of the system, potentially influencing subsequent observations. The methods described in this report avoid all these limitations by providing an increased field of view, improved image quality, and no disturbance to the flow field.

Variations in the extent and nature of protein adsorption, particularly fibrinogen, would be expected to be related to the variation in platelet adhesion observed between materials. Ye et al. previously incubated Ti6Al4V and MPC-Ti6Al4V in buffer solution containing ovine fibrinogen and quantified surface protein adsorption [4]. It was found that MPC-Ti6Al4V had significantly less fibrinogen adsorption than the unmodified titanium alloy [4], which could explain the marked reductions in platelet adhesion observed in this study. While it has been demonstrated that fibrinogen from plasma dominates as the blood adsorbate driving platelet adhesion on artificial surfaces [42], a key factor is the conformational state of the adsorbed fibrinogen and not necessarily the total amount of adsorbed protein [43]. The employment of monoclonal antibodies specific for platelet binding sites on fibrinogen would be a means to investigate whether the trends in platelet adhesion observed in this study for the various opaque surfaces could be directly related back to fibrinogen adsorption and orientation on the surface [43].

In this study, all materials exhibited an inverse relationship between wall shear rate and area of platelet coverage. Previous studies that investigated the effect of shear rate on platelet adhesion onto highly thrombogenic surfaces such as type I collagen or tissue factor showed that platelet deposition increased directly with shear rate [44, 45]. This may simply be due to higher shear rates being associated with greater platelet transport to these surfaces, which are highly platelet reactive [26, 46]. For the surfaces used in this study, the reduced platelet deposition at higher wall shear rates could be explained by shorter periods of interaction between near-wall platelets and surface-bound ligands or greater drag forces on platelets forming transient surface bonds [26, 46]. The results suggest that reducing device regions under a low wall shear rate may aid in lowering device thrombogenicity. Of particular note was the 23-fold drop in platelet coverage observed with the SiC samples at the end of the 5 min perfusion. While the results indicate less than 1% surface area coverage at the 1000 sec^{-1} wall shear rate, the videos show transient thrombotic deposition that embolizes quickly before larger thrombi can form. This is a qualitative observation that was unable to be analyzed quantitatively. While the discrete time point results suggest that SiC is less thrombogenic than Ti6Al4V at this wall shear rate, the accompanying real-time video suggests that SiC has material properties that encourage embolization and may present a clinical risk should the phenomenon occur in vivo and allow the shedding of emboli large enough to trigger tissue ischemia. Hoffman et al. reported similar material properties with hydrogel coatings where blood-contacting materials implanted in animals would lack obvious deposition onto the test surfaces at the time of explant, but where the animals had infarcts in tissue beds distal to the hydrogels [47].

Trial and error approaches to materials selection and flow path design may be used by device manufacturers in an effort to reduce thrombogenicity complications. Such methods are time-consuming and expensive, with often unpredictable outcomes. Computational models have been developed to reduce the time and cost of designing and producing safe, effective blood-wetted devices [48–52]. Flamm et al [52] performed a multiscale simulation of platelet deposition onto collagen under flow. The images produced from this simulation were visually similar to the real-time images of platelet deposition onto Ti6Al4V in the current report, suggesting that this computational model might also be applicable to synthetic biomaterials. The data collected form this study could be used to advance the accuracy and utility of such predictive models of thrombosis in blood-wetted cardiovascular devices.

An obvious limitation to this study is its acute, *in vitro* nature. Test materials were subjected to blood analogue perfusion for five min, whereas the tested materials would be implanted for much longer periods of time. However, when screening an array of alternative materials for *in vivo* testing, those forming large thrombi or experiencing substantial embolization acutely might be eliminated in favor of less reactive alternatives. A possible alternative to using a single-pass experiment would be utilizing a recirculating flow loop. This would allow for longer perfusion times and increase individual platelet interactions with the material surface through multiple passes. However, the blood would also contact larger areas of non-test surfaces, introducing artifact in the system.

Another potential limitation in this study is the use of a dilute suspension of red blood cells (25% hematocrit). Although this is lower than the average hematocrit for healthy individuals, it is not atypical for patients implanted with VADs [53]. Sodium citrate was used to limit the platelet activation caused by the blood draw. This may have reduced bulk phase platelet activation and microaggregate formation during the experiment. Heparin could have been used to mimic the anticoagulants given to VAD patients; however, studies have shown that the *in vitro* use of heparin as an anticoagulant can result in a greater incidence of spontaneous platelet aggregation and activation when compared to sodium citrate [54, 55].

When RBC ghosts are prepared, the majority of their contents are released and replaced with a saline solution. Thus RBC ghosts contain markedly less adenosine diphosphate (ADP) when compared to native RBCs, raising concerns that they may not be a suitable model, since this platelet agonist could not be released as in the native RBCs. However, because the flow produced in the flow chamber is steady laminar flow and the wall shear rates to which the RBCs are exposed are physiological, there should be limited hemolysis or shear-induced ADP release.

A final limitation of note is that thrombus growth in the vertical direction and total platelet deposition was not quantified in these experiments. While earlier work has shown that the overall fluorescence intensity of the microscopic field of view might be used as a correlate of platelet deposition, [56] this was not possible with the current system. High background fluorescence from free quinacrine dihydrochloride in the clear perfusate was a confounding factor here, as was the lack of opaque RBCs to quench this free fluorophore. The temporal measurements of platelet adhesion should thus be considered in the context of the video data, which demonstrate that the platelet adhesion was reflective of the formation of distinct thrombi. The observation that the thrombi grow in elliptical patterns in the downstream direction is in agreement with similar studies investigating mural thrombus formation [57]. These thrombi would presumably also grow in the vertical direction as later arriving platelets preferred to join existing thrombi rather than adhere to patches of the surface where platelets were not adhering.

Conclusion

Mixing of RBC ghosts with fluorescently-labeled platelets creates an effective blood analogue with which the acute thrombogenicity of opaque blood-contacting materials can be assessed. This method was used to evaluate several materials under consideration for utilization in blood-contacting medical devices, such as VADs. The reduced platelet deposition at elevated wall shear rate that was observed in this study suggests that the blood biocompatibility of VADs might be improved by minimizing the areas of low shear blood contact. Furthermore, this technique revealed that MPC-TI6AL4V and ZTA have improved thromboresistance when compared to Ti6Al4V and, thus, may be alternatives for consideration in future VAD designs.

Supplementary Material

Refer to Web version on PubMed Central for supplementary material.

Acknowledgments

The assistance of Dr. Richard Miller, Amanda Sivek, Salim Olia, Drake Pedersen, and Steven Sklar in sample processing and data collection are acknowledged. We thank Dan McKeel for his assistance in designing the parallel plate flow chamber and Dr. Sang-Ho Ye for providing the MPC-TI6AL4V coated samples. We thank Jackie Chen and Carnegie Mellon University's Center for Bioimage Informatics for their assistance in developing the image analysis MatLab program, and the University of Pittsburgh's Center for Biological Imaging for use of imaging facilities.

Support was provided in part by the Cardiovascular Bioengineering Training Program (NIH Training Grant T32-HL076124), Cellular Approaches to Tissue Engineering and Regenerative Medicine (CATER, NIH Training Grant T32-EB001026), ARCS Foundation, NIH Contract No. HHSN268200448192C, NIH Grant R01 HL089456-01, and the McGowan Institute for Regenerative Medicine.

References

1. Li S, Henry JJ. Nonthrombogenic approaches to cardiovascular bioengineering. Annu Rev Biomed Eng. 2011; 13:451–75. [PubMed: 21639778]
2. de Mel A, Cousins BG, Seifalian AM. Surface modification of biomaterials: a quest for blood compatibility. Int J Biomater. 201210.1155/2012/707863
3. Sin DC, Kei HL, Miao X. Surface coatings for ventricular assist devices. Expert Rev Med Devices. 2009; 6:51–60. [PubMed: 19105780]
4. Ye SH, Johnson CA Jr, Woolley JR, Murata H, Gamble LJ, Ishihara K, et al. Simple surface modification of a titanium alloy with silanated zwitterionic phosphorylcholine or sulfobetaine modifiers to reduce thrombogenicity. Colloids Surf B Biointerfaces. 2010; 79:357–64. [PubMed: 20547042]
5. Schaub RD, Kameneva MV, Borovetz HS, Wagner WR. Assessing acute platelet adhesion on opaque metallic and polymeric biomaterials with fiber optic microscopy. J Biomed Mater Res. 2000; 49:460–8. [PubMed: 10602079]
6. Fitzpatrick JR III, Woo YJ. Mechanical Circulatory Assistance. Circ J. 2011; 75:38–46. [PubMed: 21150126]
7. Eckman PM, John R. Bleeding and thrombosis in patients with continuous-flow ventricular assist devices. Circulation. 2012; 125:3038–47. [PubMed: 22711669]
8. Kirklin JK, Naftel DC, Kormos RL, Stevenson LW, Pagani FD, Miller MA, et al. Fifth INTERMACS annual report: risk factor analysis from more than 6,000 mechanical circulatory support patients. J Heart Lung Transplant. 2013; 32:141–56. [PubMed: 23352390]
9. Starling RC, Moazami N, Silvestry SC, Ewald G, Rogers JG, Milano CA, et al. Unexpected Abrupt Increase in Left Ventricular Assist Device Thrombosis. N Engl J Med. 2014; 370(1):33–40. [PubMed: 24283197]
10. Stulak JM, Lee D, Haft JW, Romano MA, Cowger J, Park SJ, et al. Gastrointestinal bleeding and subsequent risk of thromboembolic events during support with a left ventricular assist device. J Heart Lung Transplant. 201310.1016/j.healun.2013.07.020
11. Dion I, Baquey C, Monties JR, Havlik P. Haemocompatibility of Ti6A14V alloy. Biomaterials. 1993; 14:122–6. [PubMed: 8435455]
12. Riedel NA, Smith BS, Williams JD, Popat KC. Improved thrombogenicity on oxygen etched Ti6Al4V surfaces. Mater Sci Eng, C. 2012; 32:1196–203.
13. Walkowiak-Przybylo M, Klimek L, Okroj W, Jakubowski W, Chwilka M, Czajka A, et al. Adhesion, activation, and aggregation of blood platelets and biofilm formation on the surfaces of titanium alloys Ti6Al4V and Ti6Al7Nb. J Biomed Mater Res A. 2012; 100:768–75. [PubMed: 22238248]

14. Savage B, Saldívar E, Ruggeri ZM. Initiation of platelet adhesion by arrest onto fibrinogen or translocation on von Willebrand factor. Cell. 1996; 84(2):289–97. [PubMed: 8565074]
15. Dise CA, Burch JW, Goodman DB. Direct interaction of mepacrine with erythrocyte and platelet membrane phospholipid. J Biol Chem. 1982; 257(9):4701–4. [PubMed: 6802839]
16. Schwoch G, Passow H. Preparation and properties of human erythrocyte ghosts. Mol Cell Biochem. 1973; 2:197–218. [PubMed: 4272551]
17. Aarts PA, van den Broek SA, Prins GW, Kuiken GD, Sixma JJ, Heethaar RM. Blood platelets are concentrated near the wall and red blood cells, in the center in flowing blood. Arteriosclerosis. 1988; 8:819–24. [PubMed: 3196226]
18. Goldsmith HL, Bell DN, Braovac S, Steinberg A, McIntosh F. Physical and Chemical Effects of Red Cells in the Shear-induced Aggregation of Human Platelets. Biophys J. 1995; 69:1584–95. [PubMed: 8534829]
19. Bozzo J, Tonda R, Hernández MR, Alemany M, Galán AM, Ordinas A, Escolar G. Comparison of the effects of human erythrocyte ghosts and intact erythrocytes on platelet interactions with subendothelium in flowing blood. Biorheology. 2001; 38:429–37. [PubMed: 12016325]
20. Johnson CA Jr, Vandenberghe S, Daly AR, Woolley JR, Snyder ST, Verkaik JE, et al. Biocompatibility assessment of the first generation PediaFlow pediatric ventricular assist device. Artif Organs. 2011; 35:9–21. [PubMed: 20626737]
21. Kent NJ, Basabe-Desmonts L, Meade G, MacCraith BD, Corcoran BG, Kenny D, et al. Microfluidic device to study arterial shear-mediated platelet-surface interactions in whole blood: reduced sample volumes and well-characterised protein surfaces. Biomed Microdevices. 2010; 12:987–1000. [PubMed: 20652753]
22. Song X, Throckmorton AL, Wood HG, Antaki JF, Olsen DB. Quantitative Evaluation of Blood Damage in a Centrifugal VAD by Computational Fluid Dynamics. J Fluids Eng. 2004; 126(3): 410–18.
23. Wu J, Paden BE, Borovetz HS, Antaki JF. Computational fluid dynamics analysis of blade tip clearances on hemodynamic performance and blood damage in a centrifugal ventricular assist device. Artif Organs. 2010; 34(5):402–11. [PubMed: 19832736]
24. Zhang Y, Zhan Z, Gui XM, Sun HS, Zhang H, Zheng Z, Zhou JY, Zhu XD, Li GR, Hu SS, Jin DH. Design optimization of an axial blood pump with computational fluid dynamics. ASAIO J. 2008; 54(2):150–5. [PubMed: 18356647]
25. Johnson CA Jr, Snyder TA, Woolley JR, Wagner WR. Flow cytometric assays for quantifying activated ovine platelets. Artif Organs. 2008; 32:136–45. [PubMed: 18005275]
26. Sorensen EN, Burgreen GW, Wagner WR, Antaki JF. Computational simulation of platelet deposition and activation: II. Results for Poiseuille flow over collagen. Ann Biomed Eng. 1999; 27:449–58. [PubMed: 10468229]
27. Deible CR, Petrosko P, Johnson PC, Beckman EJ, Russell AJ, Wagner WR. Molecular barriers to biomaterial thrombosis by modification of surface proteins with polyethylene glycol. Biomaterials. 1999; 20:101–9. [PubMed: 10022779]
28. Lei L, Li C, Yang P, Huang N. Photo-immobilized heparin micropatterns on Ti–O surface: preparation, characterization, and evaluation in vitro. J Mater Sci. 2011; 46:6772–82.
29. Godo MN, Sefton MV. Characterization of transient platelet contacts on a polyvinyl alcohol hydrogel by video microscopy. Biomaterials. 1999; 20:1117–26. [PubMed: 10382827]
30. Otto M, Franzen A, Hansen T, Kirkpatrick CJ. Modification of human platelet adhesion on biomaterial surfaces by protein preadsorption under static and flow conditions. J Mater Sci Mater Med. 2004; 15:35–42. [PubMed: 15338589]
31. Zhao R, Kameneva MV, Antaki JF. Investigation of platelet margination phenomena at elevated shear stress. Biorheology. 2007; 44:161–77. [PubMed: 17851165]
32. Xu C, Wootton DM. Platelet near-wall excess in porcine whole blood in artery-sized tubes under steady and pulsatile flow conditions. Biorheology. 2004; 41:113–25. [PubMed: 15090680]
33. Tokarev AA, Butylin AA, Ataullakhanov FI. Platelet adhesion from shear blood flow is controlled by near-wall rebounding collisions with erythrocytes. Biophys J. 2011; 100:799–808. [PubMed: 21320422]

34. Kim S, Ong PK, Yalcin O, Intaglietta M, Johnson PC. The cell-free layer in microvascular blood flow. Biorheology. 2009; 46:181–9. [PubMed: 19581726]
35. Sherwood JM, Dusting J, Kaliviotis E, Balabani S. The effect of red blood cell aggregation on velocity and cell-depleted layer characteristics of blood in a bifurcating microchannel. Biomicrofluidics. 2012; 6:24119. [PubMed: 23667411]
36. Baskurt OK, Meiselman HJ. Blood rheology and hemodynamics. Semin Thromb Hemost. 2003; 29:435–50. [PubMed: 14631543]
37. Szarvas M, Oparaugo P, Udvardy ML, Toth J, Szanto T, Daroczi L, et al. Differential platelet deposition onto collagen in cone-and-plate and parallel plate flow chambers. Platelets. 2006; 17:185–90. [PubMed: 16702046]
38. Wang S, Gupta AS, Sagnella S, Barendt PM, Kottke-Marchant K, Marchant RE. Biomimetic fluorocarbon surfactant polymers reduce platelet adhesion on PTFE/ePTFE surfaces. J Biomater Sci Polym Ed. 2009; 20:619–35. [PubMed: 19323880]
39. Uchida M, Ito A, Furukawa KS, Nakamura K, Onimura Y, Oyane A, et al. Reduced platelet adhesion to titanium metal coated with apatite, albumin-apatite composite or laminin-apatite composite. Biomaterials. 2005; 26:6924–31. [PubMed: 15967494]
40. Milner KR, Snyder AJ, Siedlecki CA. Sub-micron texturing for reducing platelet adhesion to polyurethane biomaterials. J Biomed Mater Res A. 2006; 76:561–70. [PubMed: 16278867]
41. Furukawa KS, Nakamura K, Onimura Y, Uchida M, Ito A, Yamane T, et al. Quantitative analysis of human platelet adhesions under a small-scale flow device. Artif Organs. 2010; 34:295–300. [PubMed: 20420611]
42. Tsai WB, Grunkemeier JM, McFarland CD, Horbett TA. Platelet adhesion to polystyrene-based surfaces preadsorbed with plasmas selectively depleted in fibrinogen, fibronectin, vitronectin, or von Willebrand's factor. J Biomed Mater Res. 2002; 60:348–359. [PubMed: 11920657]
43. Tsai WB, Grunkemeier JM, Horbett TA. Variations in the ability of adsorbed fibrinogen to mediate platelet adhesion to polystyrene-based materials: A multivariate statistical analysis of antibody binding to the platelet binding sites of fibrinogen. J Biomed Mater Res A. 2003; 67A:1255–1268. [PubMed: 14624512]
44. Colace T, Falls E, Zheng XL, Diamond SL. Analysis of morphology of platelet aggregates formed on collagen under laminar blood flow. Ann Biomed Eng. 2011; 39:922–9. [PubMed: 20949319]
45. Tonda R, Lopez-Vilchez I, Navalon F, Pino M, Hernandez MR, Escolar G, et al. Platelets interact with tissue factor immobilized on surfaces: effects of shear rate. Eur J Clin Invest. 2008; 38:34–42. [PubMed: 18173549]
46. Sorensen EN, Burgreen GW, Wagner WR, Antaki JF. Computational simulation of platelet deposition and activation: I. Model development and properties. Ann Biomed Eng. 1999; 27:436–48. [PubMed: 10468228]
47. Hoffman AS, Cohn D, Hanson S, Harker L, Horbett T, Ratner B, et al. Application of radiation-grafted hydrogels as blood-contacting biomaterials. Radiat Phys Chem. 1983; 22:267–83.
48. Hund SJ, Antaki JF. An extended convection diffusion model for red blood cell-enhanced transport of thrombocytes and leukocytes. Phys Med Biol. 2009; 54:6415–35. [PubMed: 19809124]
49. Hund SJ, Antaki JF, Massoudi M. On the Representation of Turbulent Stresses for Computing Blood Damage. Int J Eng Sci. 2010; 48:1325–31. [PubMed: 21318093]
50. Goodman PD, Barlow ET, Crapo PM, Mohammad SF, Solen KA. Computational Model of Device-Induced Thrombosis and Thromboembolism. Ann Biomed Eng. 2005; 33:780–97. [PubMed: 16078618]
51. Bluestein D, Girdhar G, Einav S, Slepian MJ. Device thrombogenicity emulation: a novel methodology for optimizing the thromboresistance of cardiovascular devices. J Biomech. 2013; 46:338–44. [PubMed: 23219278]
52. Flamm MH, Colace TV, Chatterjee MS, Jing H, Zhou S, Jaeger D, et al. Multiscale prediction of patient-specific platelet function under flow. Blood. 2012; 120:190–8. [PubMed: 22517902]
53. Woolley JR, Teuteberg JJ, Bermudez CA, Bhama JK, Lockard KL, Kormos RL, et al. Temporal Leukocyte Numbers and Granulocyte Activation in Pulsatile and Rotary Ventricular Assist Device Patients. Artif Organs. 201310.1111/aor.12200

54. Golański J, Pietrucha T, Baj Z, Greger J, Watala C. Molecular insights into the anticoagulant-induced spontaneous activation of platelets in whole blood-various anticoagulants are not equal. Thromb Res. 1996; 83:199–216. [PubMed: 8840462]

55. Harding SA, Din JN, Sarma J, Jessop A, Weatherall M, Fox KA, et al. Flow cytometric analysis of circulating platelet-monocyte aggregates in whole blood: Methodological considerations. Thromb Haemost. 2007; 98(2):451–6. [PubMed: 17721630]

56. Wagner WR, Hubbell JA. Local thrombin synthesis and fibrin formation in an in vitro thrombosis model result in platelet recruitment and thrombus stabilization on collagen in heparinized blood. J Lab Clin Med. 1990; 116(5):636–50. [PubMed: 2104522]

57. Jackson SP. The growing complexity of platelet aggregation. Blood. 2007; 109:5087–95. [PubMed: 17311994]

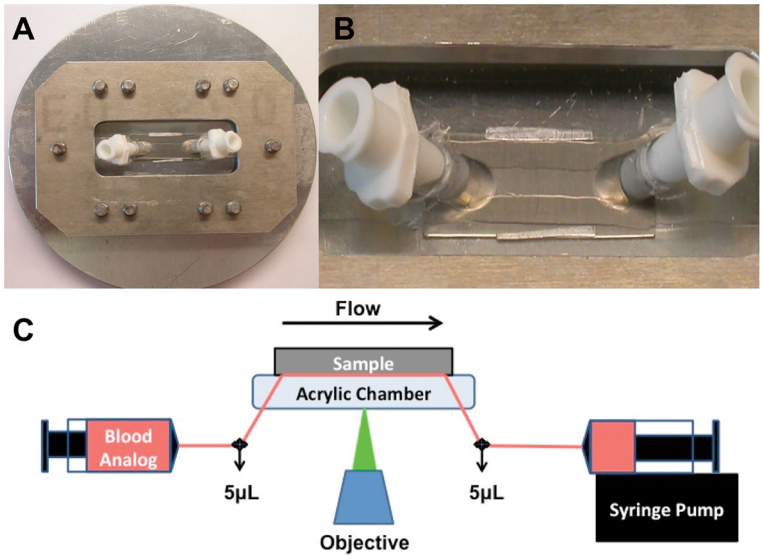

Figure 1.

Parallel plate flow chamber and experimental set up. A) The circular metallic piece and rectangle were secured around the flow chamber with screws. B) The flow path was formed from a silicon gasket. Thin aluminum shim stock can be seen along the length of either side of the silicone gasket to ensure a precise chamber height. C)The blood analogue was perfused through the chamber and across the sample for 5 min. Images were acquired, in real time, 4mm from the inlet by a CCD camera. The transparent blood analogue and long working distance objective allowed for real time visualization of adherent fluorescent platelets through the flow path onto the opaque test surface.

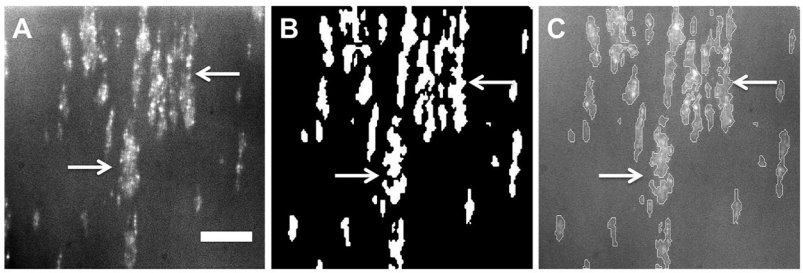

Figure 2.

Image analysis to quantify the percent platelet surface coverage. A) Original fluorescent image of platelets adhered to SiC after 5 min of perfusion, B) binary image rendered by the MatLab program, C) original fluorescent image overlaid with the outline of the binary image. Scale bar = 40 μm

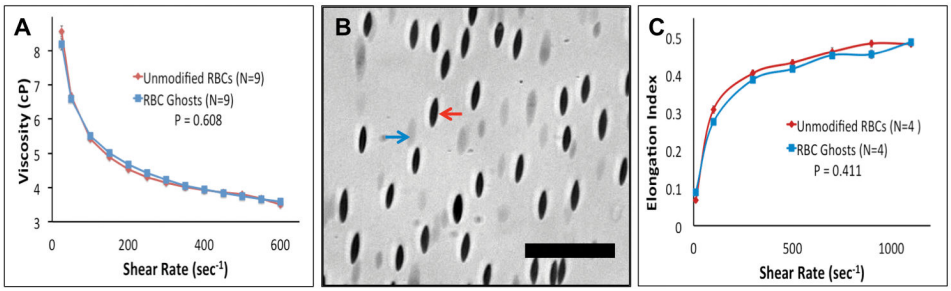

Figure 3.

A) Comparing the viscosity of native and ghost RBCs in human plasma at a matched hematocrit of 27%. B) Mixture of native and ghost RBCs subjected to a wall shear rate of 1100 sec^{-1}. Red and blue arrows indicate a native and ghost RBC respectively. Scale bar = 40 μm. C) Deformability of native and ghost RBCs.

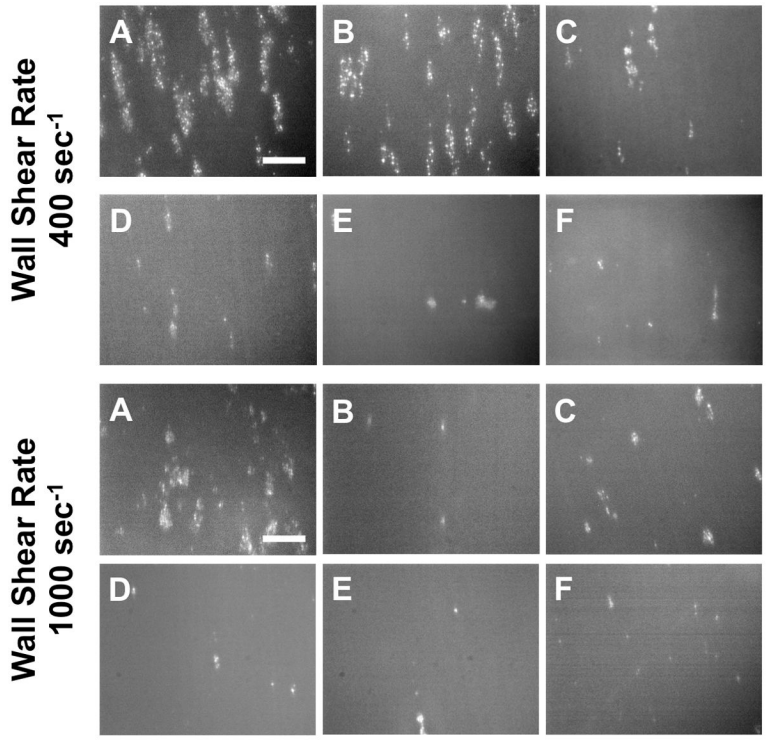

Figure 4.

Representative fluorescent images of platelets adhered to A) Ti6Al4V, B) SiC, C) Al_2O_3, D) YZTP, E) ZTA, and F) MPC-TI6AL4V after 5 min of perfusion. Scale bar = 40 μm.

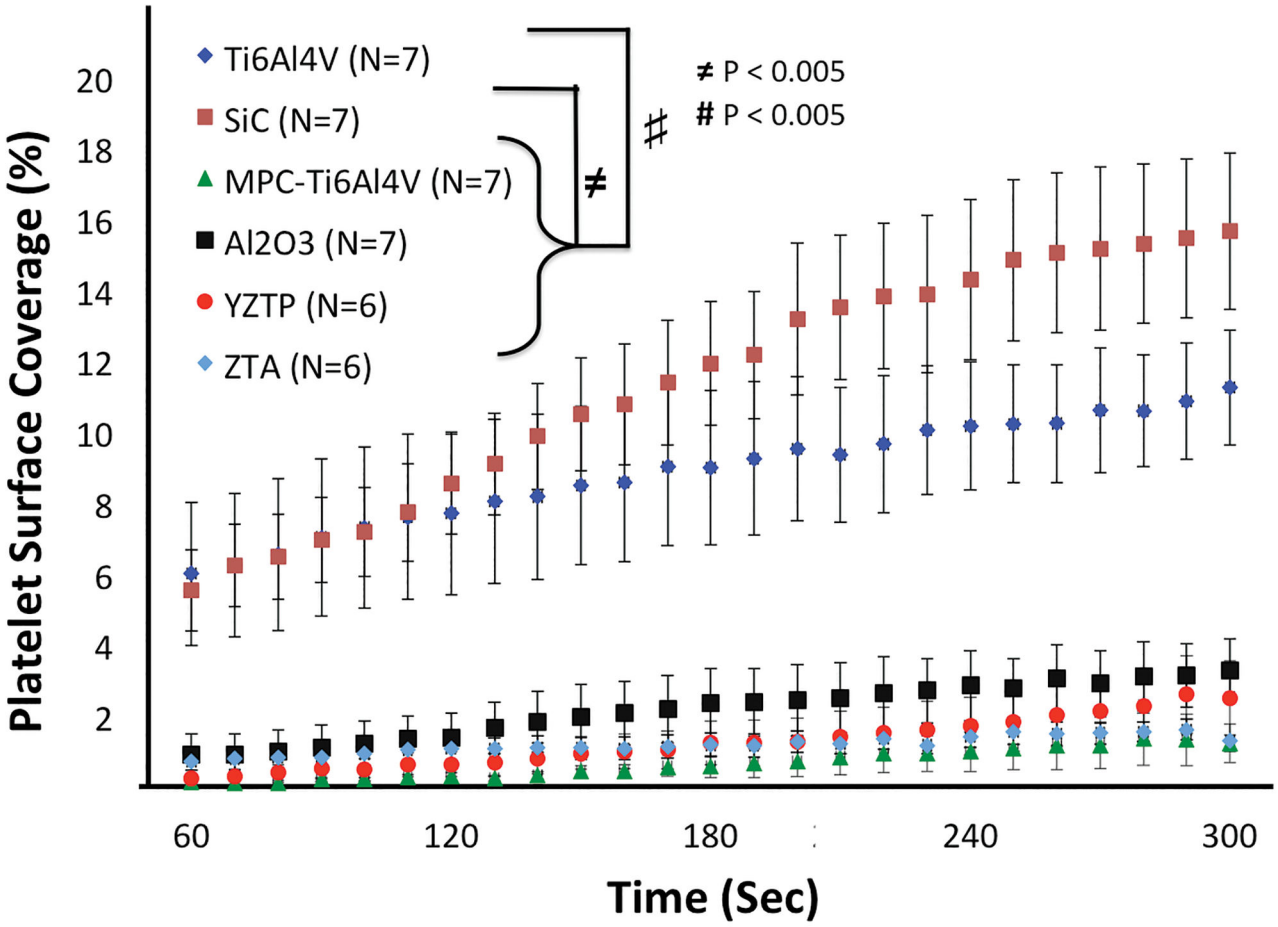

Figure 5.

Acute platelet adhesion on test materials perfused at a wall shear rate of 400 sec^{-1}. Images were acquired at 4mm distance from the inlet of the parallel plate flow chamber.

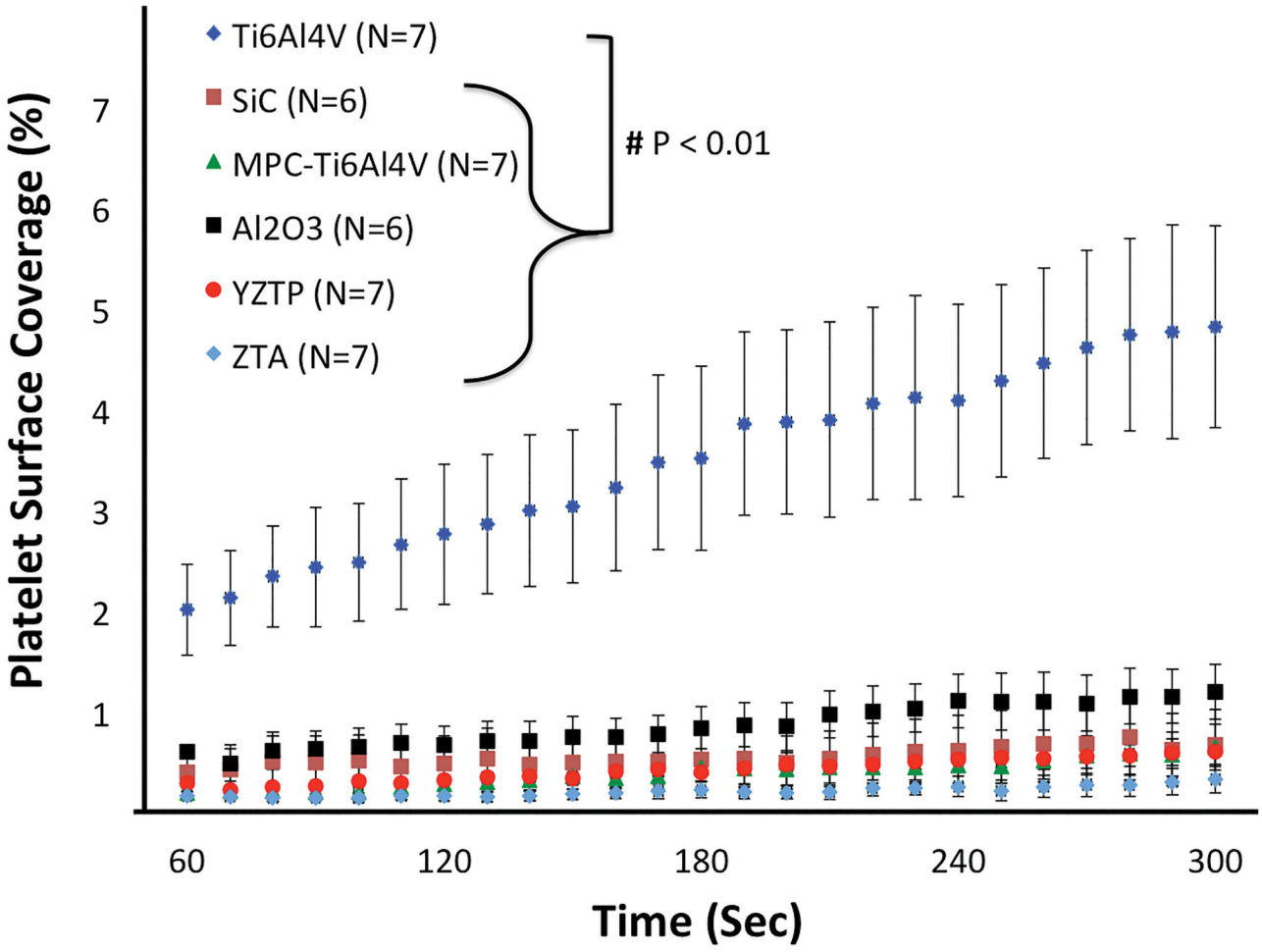

Figure 6.

Acute platelet adhesion on test materials perfused at a wall shear rate of 1000 sec^{-1}. Images were acquired 4mm from the inlet of the parallel plate flow chamber.

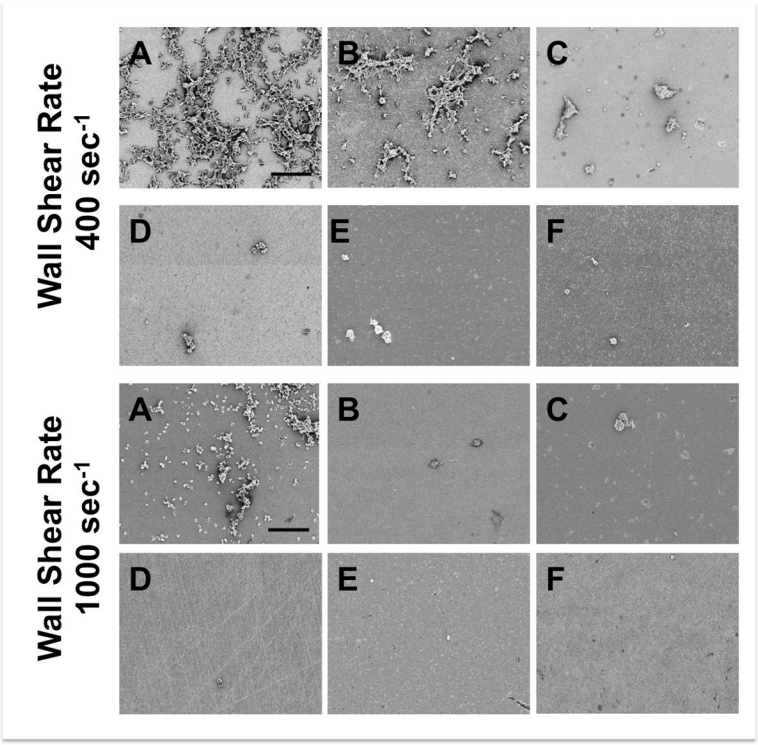

Figure 7.

Representative scanning electron micrographs of platelets adhered to A) Ti6Al4V, B) SiC, C) Al_2O_3, D) YZTP, E) ZTA, and F) MPC-TI6AL4V after 5 min of perfusion. Scale bar = 40 μm.